New Advances in Nanocrystalline Apatite Colloids Intended for Cellular Drug Delivery

Amal Bouladjine, Ahmed Al-Kattan, Pascal Dufour, Christophe Drouet

New Advances in Nanocrystalline Apatite Colloids Intended for Cellular Drug Delivery

Amal Bouladjine, Ahmed Al-Kattan, Pascal Dufour, and Christophe Drouet*

CIRIMAT Carnot Institute, University of Toulouse, CNRS/INPT/UPS, ENSIACET, 118 route de Narbonne, 31077 Toulouse, France

Intracellular drug delivery using colloidal biomimetic calcium phosphate apatites as nanocarriers is a seducing concept. However, the colloid preparation to an industrial scale requires the use of easily handled raw materials as well as the possibility to tailor the nanoparticles size. In this work, the stabilization of the colloids was investigated with various biocompatible agents. Most interestingly, nanoscale colloids were obtained without the need for toxic and/or hazardous raw materials. Physico-chemical characteristics were investigated by chemical analyses, dynamic light scattering, FTIR/Raman spectroscopies, XRD, and electron microscopy. A particularly promising colloidal system associates biomimetic apatite stabilized with a natural phospholipid moiety (AEP_r, 2-aminoethylphosphoric acid). Complementary data described such colloids as apatite nanocrystals covered with surface $Ca^{2+}(AEP_r^-)_2$ complexes involving "supernumerary" Ca^{2+} ions. The effects of the concentration in AEPr, synthesis temperature, duration of aging in solution, pH, and sonication were followed, showing that it is possible to modulate the mean size of the nanoparticles, typically in the range 30−100 nm. The perfect biocompatibility of such colloids allied to the possibility to prepare them from innocuous compounds shows great promise for intracellular drug delivery.

1. Introduction

The treatments of cell-related diseases such as cancer or genetic disorders are in constant evolution, and therapeutic routes based on intracellular drug delivery are among the most promising clinical paths.[1] In this approach, drugs can advantageously be associated to a carrier, which can protect them and significantly orient their delivery in the organism.[2,3] Also, the carrier can be coupled with a cell-targeting agent (antibody, peptide, folic acid, etc.) for addressing specifically the diseased cells leading to greatly increased treatment efficacy.[4,5]

Such drug carriers are generally administered via intravenous injection. A recurrent concern is the need for small enough carriers capable of being ultimately internalized by diseased cells, generally by way of endocytosis. Indeed, in addition to essential biochemical considerations linked to the biology of the cell membrane and the chemical nature of the drug carrier, several authors have pointed out the major impact of the carrier size on drug delivery efficacy.[5−7] Nowadays, the generally accepted upper size limit for favorable intracellular drug delivery lies around 100 nm, which emphasizes again the potential impact of nanobiotechnologies in medicine.[8]

In this context, the search for adapted nanosized systems for the setup of innovative and efficient drug delivery solutions is in continual development. So far, a number of prospective drug carriers have been envisioned including (but not limited to) metal nanoparticles (e.g., gold), polymer-based nanoparticles or nanocapsules, and liposomes.[9] Some of these systems have been clinically tested, and primary assessments of efficiency and limitations were drawn. Recent progress in liposome systems have in particular led to numerous reports, and significant clinical advances over existing drug carriers have been acknowledged.[10] However, the stability of liposomes in contact with plasma proteins as well as the difficulty obtaining sustained cytosolic delivery of the therapeutic agent still represent some obstacles to some ultimate development.[11]

Besides this constraint on carrier size, in relation to the potential ease of internalization by cells, the probability that the carrier can actually reach the cells has to also be considered in view of successful drug delivery. This is in particular linked to the reticulo-endothelial system (RES), which includes macrophage cells (e.g., Kupffer cells in the liver) supposed to clear the bloodstream from circulating, potentially harmful foreign entities. In order to increase the residence time of a drug carrier in the vasculature, it should thus primarily be rendered rather unnoticeable to such "clearing" cells.

One solution to this problem was obtained by functionalizing the surface of drug carriers with macromolecules in order to prevent, by steric hindrance, the preliminary adsorption of opsonin proteins. Indeed, opsonin adsorption is known to make foreign circulating entities detectable by macrophages. This method was for example used in the case of liposomes by surface grafting of poly(ethylene glycol) (PEG) macromolecules.[3] However, despite the longer residence time in blood circulation observed for such PEG-treated drug carriers, several issues related to the use of such macromolecules exist and limit their

*Corresponding author. Dr. Christophe Drouet, Ph.D. Phone: +33 5 62 88 57 60. Fax: +33 5 62 88 57 73. E-mail: christophe.drouet@ensiacet.fr.

(1) Bareford, L. M.; Swaan, P. W. *Adv. Drug Delivery Rev.* **2007**, *59*, 748–758.
(2) Alonso, M. J. *Biomed. Pharmacother.* **2004**, *58*, 168–172.
(3) Couvreur, P.; Gref, R.; Andrieux, K.; Malvy, C. *Prog. Solid State Chem.* **2006**, *34*, 231–235.
(4) Blay, J. Y. *Bull. Cancer* **2006**, *93*, 799–804.
(5) Moghimi, S. M.; Hunter, A. C.; Murray, J. C. *Pharmacol. Rev.* **2001**, *53*, 283–318.
(6) Seijo, B.; Fattal, E.; Roblot-Treupel, L.; Couvreur, P. *Int. J. Pharm.* **1990**, *62*, 1–7.
(7) Moghimi, S. M.; Bonnemain, B. *Adv. Drug Delivery Rev.* **1999**, *37*, 295–312.
(8) Orive, G.; Hernandez, R. M.; Rodriguez Gascon, A.; Dominguez-Gily, A.; Pedraz, J. L. *Curr. Opin. Biotechnol.* **2003**, *14*, 659–664.
(9) Breunig, M.; Bauer, S.; Goepferich, A. *Eur. J. Pharm. Biopharm.* **2008**, *68*, 112–128.
(10) Haley, B.; Frenkel, E. *Urologic Oncology: Semin. Orig. Invest.* **2008**, *26*, 57–64.
(11) Vasir, J. K.; Labhasetwar, V. *Adv. Drug Delivery Rev.* **2007**, *59*, 718–728.

eventual interest: First, the high polydispersity of macromolecules like PEG poses a potential problem, which can lead to a population of drug conjugates with possibly varying biological properties (e.g., regarding immunogenicity, residence times).[12] Second, as for other polymers, the excretion of PEG from the body can prove problematic, especially at high molecular weights where the macromolecules can accumulate in the liver leading to the "macromolecular syndrome".[12] Third, the kidney excretion limit for PEG is not easy to determine, partly due to its high water coordination leading to colossal hydrodynamic volumes.[12]

Another way to increase the residence time of drug carriers in the vasculature is by further decreasing their size,[5] especially under the 100 nm limit mentioned above. Indeed, nanoparticles become barely detectable when their size is reduced to some tens of nanometers.[7] In this case, the nanocarriers are more likely to access the diseased organs and cells by selective diffusion through blood vessels (transcytosis). This is especially remarkable since vascular endothelia exhibit a greater permeability in the vicinity of an inflammatory region or near a tumoral tissue.[13]

With all the above considerations in mind, the preparation of new generations of nanodrug carriers is in ever-growing development worldwide, and the possibility to control the carrier size below 100 nm as well as their full biocompatibility (including that of degradation products) appear nowadays as fundamental prerequisites. Besides, synthetic nanoparticles are of particular interest as they do not originate from biological sources, thus eliminating immunological or ethical issues.

The use of biomimetic systems appears a clever way to satisfy the biocompatibility criterion. In this view, nanocrystalline calcium phosphate apatites, responding to the general chemical formula $Ca_{10-x}(PO_4)_{6-x}(HPO_4)_x(OH)_{2-x}$ ($0 \le x \le 2$) are promising candidates as they are biomimetic compounds analogous to bone mineral.[14] Their physicochemical characteristics and surface state have been largely investigated in the literature, especially in view of bone regeneration applications.[15,16] The use of calcium phosphates for cellular drug delivery (e.g., for nonviral transfection applications) has led to a number of studies, and several of those were listed and commented on in a recent review-like article.[17] However, particle size control and agglomeration was often reported as an issue in the systems tested, especially for calcium phosphate−DNA hybrids.[17] More recently, colloidal suspensions of apatite nanocrystals have been prepared for the setup of nanophosphors.[18] However, this synthesis of apatite colloids was so far mostly based on precipitation from phosphoric acid (H_3PO_4) and freshly calcined calcium oxide (CaO), partly carried out under inert atmosphere to avoid rehydration of CaO, and was therefore hardly transposable to an industrial scale. Also, the handling of such starting materials was potentially hazardous.

We report in the present contribution new advances on the preparation of colloidal suspensions of biomimetic nanocrystalline apatites, starting from aqueous solutions of easily handled mineral salts. The stabilization of the colloids was investigated by surface functionalization with varying biocompatible agents. Several physicochemical characteristics of the nanoparticles, including their size and composition, were determined and the role of synthesis parameters on particle size control, in particular, was analyzed.

(12) Veronese, F. M.; Pasut, G. *Drug Discovery Today* **2005**, *10*, 1451–1458.
(13) Poznansky, M. J.; Juliano, R. L. *Pharmacol. Rev.* **1984**, *36*, 277–336.
(14) Legeros, R. Z. *Prog. Cryst. Growth Charact.* **1981**, *4*, 1–45.
(15) Cazalbou, S.; Eichert, D.; Ranz, X.; Drouet, C.; Combes, C.; Harmand, M. F.; Rey, C. *J. Mater. Sci.: Mater. Med.* **2005**, *16*, 405–409.
(16) Rey, C.; Combes, C.; Drouet, C.; Sfihi, H.; Barroug, A. *Mater. Sci. Eng., C* **2007**, *27*, 198–205.
(17) Xu, Z. P.; Zeng, Q. H.; Lu, G. Q.; Yu, A. B. *Chem. Eng. Sci.* **2006**, *61*, 1027–1040.
(18) Lebugle, A.; Pelle, F.; Charvillat, C.; Rousselot, I.; Chane-Ching, J. Y. *Chem. Commun.* **2006**, 606–608.

2. Materials and Methods

2.1. Synthesis. A reference noncolloidal calcium phosphate apatite sample, referred to as "hap-ref", was synthesized by coprecipitation obtained by mixing an aqueous solution of calcium nitrate (3.12 M) and an aqueous solution of ammonium hydrogenphosphate (1.04 M). The total volume was 12.5 mL. Reagent-grade reactants exempt of impurities (such as Mg^{2+} ions) were selected for this work. An excess of calcium ions (initial Ca/P molar ratio of 3) and a starting alkaline pH value, set to 9 (unless otherwise specified) by addition of ammonia, were chosen here in order to favor the formation of a hydroxylated apatite (with a limited degree of nonstoichiometry and a greater thermodynamic stability than usual biomimetic apatites). After mixing the solutions, the precipitate was stirred in a closed vial for 15 min at room temperature before being placed in an oven preset to 80 °C for a 16 h (overnight) aging step. The sample was then retrieved by centrifugation, washed with deionized water, and freeze−dried for powder analysis.

Colloidal formulations were investigated by performing the above synthesis protocol but in the presence of a dispersing (or "stabilizing") agent selected between folic acid, glutamic acid (Glu), 2-aminoethyl-phosphoric acid (AEP_r), and 2-aminoethylphosphonic acid (AEP_n), introduced in the calcium solution. For those dispersing agents, varying concentrations were studied in the range 0−1.6 M, as indicated in the text, except for folic acid for which a concentration of 0.27 mM was used (linked to a low solubility in water).

In some cases, as described in the manuscript, the duration and/or temperature of the aging step was varied to study their effect on the physicochemical characteristics of the samples. Dialysis through a cellulose tubular membrane (molecular weight cutoff: 6000−8000 Da) was used for purifying the suspensions (dialysis medium: deionized water, room temperature). In view of physicochemical analyses, part of each dialyzed suspension was sampled and freeze−dried for retrieving the particles.

2.2. Physico-Chemical Characterization. The crystal structure of the samples was investigated by powder X-ray diffraction using an Inel diffractometer CPS 120 and the monochromatic Co K_α radiation (λ_{Co} = 1.788 92 Å). The acquisition time was set to 15 h. Rietveld refinements were performed using the software *MAUD* (2.062 version, 2006).

Fourier transform infrared (FTIR) analyses were carried out on a Nicolet 5700 spectrometer, in the wavenumber range 400−4000 cm^{-1} with a resolution of 4 cm^{-1}, using the KBr pellet method. Raman spectra were recorded on a Jobin Yvon HR 800 spectrometer, with a laser excitation wavelength of 632.8 nm.

The total calcium content in the samples was measured by complexometry with EDTA. The amount of mineral phosphate (from apatite) was estimated by spectrophotometry of the colored phospho-vanado-molybdenum complex (this complex cannot form with organic phosphate groups). These techniques are customary for analyzing calcium phosphate compounds, and the estimated relative uncertainties on calcium and phosphate concentrations are evaluated at 0.5%. Elemental microanalyses for nitrogen contents were performed on a Perkin-Elmer 2400 II analyzer (relative uncertainty: 0.4%).

Granulometric data (determination of hydrodynamic radius) for the colloidal particles were obtained using a Malvern Nanosizer ZS apparatus (λ = 630 nm) by dynamic light scattering (DLS). The error on the dispersion of the data points was evaluated to 0.5%. The particle size distribution of noncolloidal apatite (in the micrometer range) was measured by laser diffraction with a Malvern Mastersizer 2000. In the text, the "particle size" refers to the median diameter "d_{50}" (dividing the particle population into two equal halves).

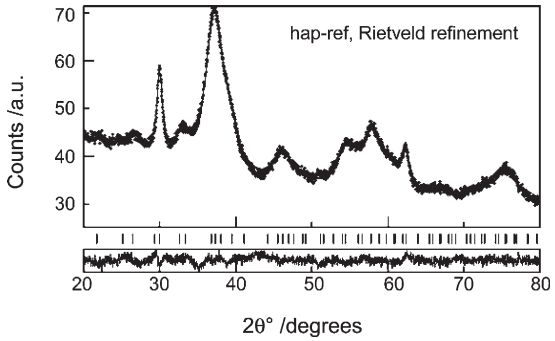

Figure 1. XRD pattern and Rietveld fit for noncolloidal reference apatite "hap-ref".

Transmission electron microscopy (TEM) micrographs were recorded for colloidal apatites on a JEOL JEM-1011 microscope, set up at an acceleration tension of 100 kV. Scanning electron microscopy (SEM) was used in the secondary electron mode (LEO 435 VP microscope, tension 15 kV) for observing the larger, noncolloidal particles of the "hap-ref" sample.

3. Results and Discussion

3.1. Noncolloidal Reference Apatite. The main objective of this work was to prepare stable colloidal suspensions of apatite nanoparticles exhibiting a controllable mean size lower than 100 nm, and starting from easily handled calcium and phosphate salts.

In a first step, a noncolloidal apatite sample (denoted "hap-ref") was precipitated in the absence of dispersing (or "stabilizing") agents, to serve as a reference. This preparation led, after heat treatment at 80 °C for 16 h, to a complete sedimentation of the particles (unstable suspension). Figure 1 reports the XRD pattern of this reference sample, as well as the Rietveld refinement curve. It shows that the particles collected by centrifugation and washed with deionized water correspond to a single apatitic phase, with a moderate crystalline state. In order to evaluate the Ca/P molar ratio of this sample, part of it was subsequently calcined at 1000 °C for 15 h. Indeed, such a heating procedure leads to the thermal decomposition of apatites $Ca_{10-x}(PO_4)_{6-x}(HPO_4)_x(OH)_{2-x}$ into stoichiometric hydroxyapatite (HAP) and β-tricalcium phosphate (β-TCP) following reaction 1

$$Ca_{10-x}(PO_4)_{6-x}(HPO_4)_x(OH)_{2-x} \rightarrow (1-x)Ca_{10}(PO_4)_6(OH)_2 + 3x\beta\text{-}Ca_3(PO_4)_2 + xH_2O \quad (1)$$

and the evaluation by XRD of the relative amounts of these two phases enables one to evaluate easily the initial Ca/P ratio (for systems exempt of organic phosphate-containing compounds).[19] In the present case, stoichiometric HAP was the only phase observable after calcination, and β-tricalcium phosphate was not detected (under the limits of the equipment). These observations therefore indicate that the initial Ca/P molar ratio of the sample hap-ref is close to that of HAP, i.e., 1.67, leading to an "x" value close to 0.

The apatite nature of this "hap-ref" sample was confirmed by FTIR spectroscopy analysis (Figure 2) where typical apatitic vibrations bands were observed, in particular with bands in the regions 800−1300 cm^{-1} and 450−630 cm^{-1} attributable, respectively, to the ν_3 and ν_4 vibration modes of phosphate groups, as well as sharp bands at 3572 and 631 cm^{-1} assignable to apatitic

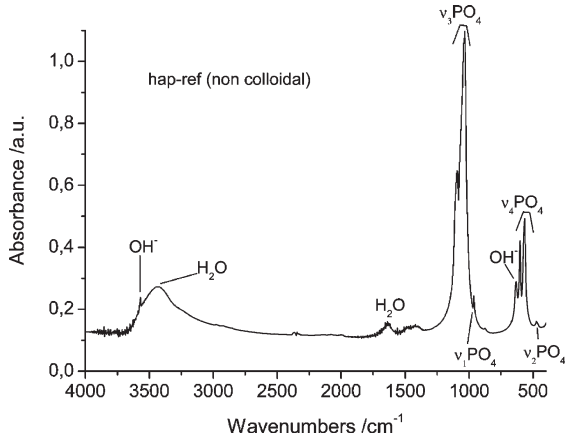

Figure 2. FTIR spectrum for noncolloidal "hap-ref" sample and assignment of absorption bands.

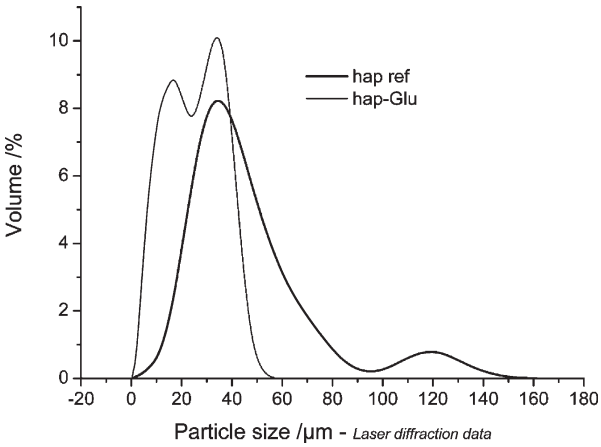

Figure 3. Particle size distribution for noncolloidal apatite "hap-ref" and apatite suspension prepared in the presence of glutamic acid (hap-Glu).

OH^- ions. In addition, a slight absorption due to traces of carbonate ions arising from dissolved atmospheric CO_2 during synthesis can also be discerned around 1500 cm^{-1}, and water bands can be seen around 3400 and 1640 cm^{-1}, which is customary with biomimetic apatites synthesized at rather low temperatures.[15,16]

The particle size distribution corresponding to the sample hap-ref, observed in the micrometer range, is reported in Figure 3. This distribution was found to be rather large and bimodal, with a main peak around 40 μm and a secondary peak centered at 120 μm. This particle size domain lies, however, far beyond the 100 nm limit value mentioned above (considered to facilitate an internalization by living cells). Therefore, various potential dispersing agents were envisaged, in the following, in order to decrease the average particle size and simultaneously stabilize the suspension from a physical point of view (preventing the sedimentation of the particles).

3.2. Colloidal Apatite Suspensions. *3.2.1. Selection of Dispersing Agents.* Apatite particles obtained from precipitation techniques are agglomerates composed of piled-up nanocrystals most probably interacting via their surface hydrated layers.[20] A reduction in size of apatite particles can therefore be anticipated (1) by decreasing the tendency of adjacent nanocrystals to

(19) Raynaud, S.; Champion, E.; Bernache-Assollant, D. *Biomaterials* **2002**, *23*, 1073–1080.

(20) Rey, C.; Combes, C.; Drouet, C.; Lebugle, A.; Sfihi, H.; Barroug, A. *Mat. Wiss. Werkstofftech.* **2007**, *38*, 1–7.

agglomerate and/or (2) to some extent by limiting the size of each individual nanocrystal (in order to obtain, in the end, smaller agglomerates).

The first option, i.e., a decreased tendency to agglomerate, can, for example, be obtained by grafting organic molecules at the surface of the crystals, in view of limiting crystal−crystal interactions due to steric hindrance. Such molecules should however show some affinity for calcium phosphates in order to interact efficiently with the apatite surface. This can be anticipated, for example, by dealing with organic molecules exhibiting ionic end-groups like carboxylates, phosphates, or phosphonates, which are known to complex surface calcium ions.[21] Besides, an electrostatic repulsive effect can be combined to the steric one by selecting molecules that exhibit additionally other ionic end-groups such as $-NH_3^+$(in addition to end-groups enabling the grafting to the particle surface).

The second option, i.e., a limitation in individual crystal size, can be envisaged by using a crystal growth inhibitor during the synthesis. Several inhibitory compounds have been identified for apatites.[21,22] Interestingly, organic molecules displaying anionic groups like carboxylate groups, phosphates, or phosphonates were shown to act also as inhibitors for apatite crystal growth.[21] In this case, the inhibitory effect is thought to be linked to a complexation of calcium ions by these anionic functional groups, therefore making Ca^{2+} less available for an interaction with phosphate ions for forming apatite.

With the above considerations in mind, the selection of (nontoxic) organic molecules exhibiting on one side a carboxylate, phosphate, or phosphonate group and on another side an $-NH_3^+$ group seemed particularly promising for acting as dispersing/stabilizing agents.

Folic acid (CAS number 59−30−3, also known as vitamin B9, a natural compound used by living cells for their normal metabolism) is one such molecule, with two carboxylic groups and one amino end-group. It is also a well-known targeting agent for accessing certain types of tumor cells (by interaction with folate receptors overexpressed on their surface),[23−26] and it was therefore of interest to check whether folic acid could play a dual role of dispersing agent and potential cell-recognition agent.

In this work, 3.4 nmol of folic acid were added in the starting mixture of solutions and the aging step was carried out with the same protocol as above. Despite the low amount of folic acid introduced here, linked to its low solubility in water, a strong destabilization of the suspension occurred leading to the sedimentation of the particles. This observation was corroborated by granulometry data pointing out (not shown) a marked agglomeration effect with a noticeable shift of the particle size distribution toward the range 300−700 μm (mean size close to 450 μm). This phenomenon might find its origin in the creation of interparticle bridging via adsorbed folic acid molecules as was evidenced earlier with polyacrylamides (internal communication).

In order to shed some light on this aspect, glutamic acid was also tested as a potential dispersing agent, by replacing folic acid in the initial aqueous mixture. Indeed, the folic acid molecule exhibits two functional parts: a "biologically-active head" which corresponds chemically to methylpterin and is the region of the molecule that is recognized by folate receptors in tumor cells, and an "attachment head" which is chemically analogous to glutamic acid and is the region where folic acid is generally attached to nanoparticles.[24−26,27]

Since glutamic acid (Glu) exhibits a greater solubility in water than folic acid, it was possible to use a greater concentration which was (arbitrarily) fixed to the same value as that of calcium ions initially present in the mixture. This value was chosen in order to provide a sufficient amount of glutamic acid so as to favor the complexation of Ca^{2+} ions and therefore limit apatite crystal growth during the aging step. However, the particle size distribution obtained in this case was still found in the micrometer range (Figure 3), although no increase in size was obtained contrarily to the experiment performed with folic acid. This point tends to indicate that the smaller, simpler molecules of glutamic acid could not lead to strong bridging effects between functionalized particles, as opposed to folic acid grafting. However, it also indicates an insufficient interaction with the apatite nanocrystals so as to limit the usual agglomeration process, which can probably be linked to the rather limited complexation power of carboxylate groups, which are in competition with phosphate ions for the complexation of calcium ions during the synthesis.

Taking into account the above findings, small organic molecules exhibiting a phosphate or phosphonate group on one side and an amino group on the other side were investigated as potential dispersing agents: in this work, we focused on 2-aminoethylphorphoric acid (AEP_r) and 2-aminoethylphorphonic acid (AEP_n) respectively. AEP_r is a phospholipid moiety, corresponding to the chemical formula $NH_2-CH_2-CH_2-O-P(O)(OH)_2$. It is perfectly biocompatible as it is encountered naturally in the composition of cell membranes,[28] and its interaction with apatites has started to be explored previously.[18] AEP_n is the phosphonic acid derivative of AEP_r, $NH_2-CH_2-CH_2-P(O)(OH)_2$, and its interaction with some living organisms has also been reported.[29] AEP_n was tested here, in parallel with AEP_r, because of the presence of a phosphonate end group, potentially capable of complexing more energetically calcium ions.

Unlike with folic acid or glutamic acid, the synthesis protocols carried out in the presence of AEP_r or AEP_n, respectively, in the initial molar proportions $AEP_r/Ca = AEP_n/Ca = 1$ led to stable colloidal suspensions and no sedimentation was observed, including after (at least) 1 year of storage at room temperature. A preliminary analysis of the granulometry of the particles in suspension indicated that their size in both cases lay in the nanometer scale, and further analyses were therefore run by measuring hydrodynamic radii using a dynamic light scattering (DLS) system. Although hydrodynamic radii generally tend to overestimate the actual particle size in such nanometer-scale systems, this deviation is here limited by the high ionic strength of the suspensions (slipping plane − containing the electrical double layer on the particle − close to the geometric surface of the particle), thus leading to acceptably exploitable particle size values.

The corresponding particle size distributions obtained are reported in Figure 4. They are represented by monomodal curves, with a median d_{50} size parameter of 29 nm for AEP_r and 26 nm for AEP_n. Very interestingly, the particle size range is found in both cases notably lower than with noncolloidal hap-ref (Figure 4) and

(21) Sallis, J. D. In *Calcium phosphates in biological and industrial systems*, Amjad, Z., Ed.; Kluwer Academic Publishers: Dordrecht, The Netherlands, 1998; p 174−191.
(22) Blumenthal, N. C. *Clin. Orthop. Rel. Res.* **1989**, *247*, 279–289.
(23) Taira, S.; Hatanaka, T.; Moritake, S.; Kai, Y.; Ichiyanagi, Y.; Setou, M. *e-J. Surf. Sci. Nanotechnol.* **2007**, *5*, 23–28.
(24) Bae, Y.; Jang, W.-D.; Nishiyama, N.; Fukushima, S.; Kataoka, K. *Mol. BioSyst.* **2005**, *1*, 242–250.
(25) Kukowska-Latallo, J. F.; Candido, K. A.; Cao, Z.; Nigavekar, S. S.; Majoros, I. J.; Thomas, T. P.; Balogh, L. P.; Khan, M. K.; Baker, J. R. *Cancer Res.* **2005**, *65*, 5317–5324.
(26) Ross, J. F.; Chaudhuri, P. K.; Ratnam, M. *Cancer* **1994**, *73*, 2432–2443.
(27) Bhalerao, K. D.; Lee, S. C.; Soboyejo, W. O.; Soboyejo, A. B. O. *J. Mater. Sci.: Mater. Med.* **2007**, *18*, 3–8.
(28) Rothfield, L.; Finkelstein, A. *Annu. Rev. Biochem.* **1968**, *37*, 463–495.
(29) Roseberg, H.; La Nauze, J. M. *Biochim. Biophys. Acta* **1967**, *141*, 79–90.

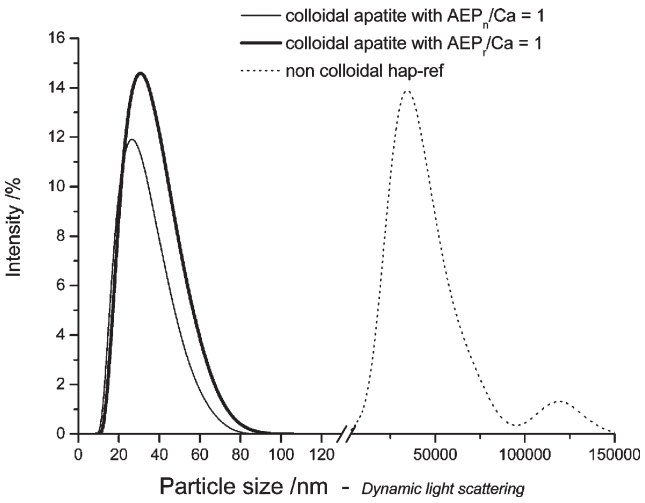

Figure 4. Particle size distribution for apatite suspensions obtained with $AEP_r/Ca = 1$ and $AEP_n/Ca = 1$, and comparison with noncolloidal apatite (hap-ref).

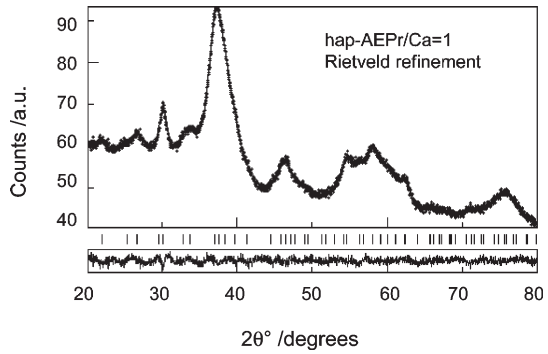

Figure 5. XRD pattern and Rietveld fit for apatite colloid starting from $AEP_r/Ca = 1$.

in particular under the 100 nm limit discussed above in view of intracellular drug delivery applications. These data can most probably be linked to the competition for Ca^{2+} between phosphate ions and AEP_r/AEP_n molecules during the synthesis, leading to a drastic decrease in size of the particles present in the final suspensions (diminished accessibility of Ca^{2+} ions for forming apatite). This effect can also be related to some electrosteric repulsion between apatite particles covered with these (charged) organic molecules. These aspects will be dealt with in more detail in the following.

Although the particle size reached in the presence of AEP_n was lower than that obtained with AEP_r, for similar concentrations, this difference appeared to be very limited. Therefore, taking into account the perfect biocompatibility of AEP_r, it was selected for the further investigations in this work.

The XRD pattern recorded for the colloidal particles obtained with the initial molar ratio $AEP_r/Ca = 1$ is reported in Figure 5. These data unveil the presence of a single apatite phase with a slightly lower crystallinity state than for noncolloidal hap-ref (see Figure 1), which is in particular noticeable in the 2θ regions 30−35° and 60−65°. This feature is thought to be due to a partial inhibitory effect of AEP_r regarding apatite crystal growth, linked to surface interactions with AEP_r molecules (limiting the crystal growth rate).

The FTIR spectrum corresponding to the above-mentioned colloidal apatite sample obtained with AEPr/Ca = 1 is reported in Figure 6. The position of the main absorption bands appeared in the regions 2900−3700 cm^{-1}, 800−1300 cm^{-1}, and 450−700 cm^{-1}, which globally coincide with absorptions observed for the reference apatitic noncolloidal sample hap-ref (see Figure 1). However, a closer examination of the two spectra indicates that bands relative to apatitic OH^- groups (normally located at 3572 and 631 cm^{-1}) are not detected in the case of the colloidal sample. The absence of a detectable amount of OH^- ions in the apatite part of the colloid was also confirmed by Raman microspectroscopy (absence of a characteristic peak at 3572 cm^{-1}). This point therefore indicates that, in this colloid, the value of "x" in the apatite chemical formula $Ca_{10-x}(PO_4)_{6-x}(HPO_4)_x(OH)_{2-x}$ is close to 2. This high value of "x", meaning an elevated amount of HPO_4^{2-} ions per unit formula, establishes the biomimetic character of this apatite phase.[16,20] The chemical formula of the apatite phase contained in the suspensions is thus close to apatitic octacalcium phosphate (apatitic OCP). This phase should not be confused with triclinic OCP which is the common form of octacalcium phosphate. In the present case indeed, the absence of a diffraction peak for the interreticular disctance $d = 18.7$ Å, characteristic of the triclinic form, was confirmed by XRD analyses. Also, the alkaline pH used during the synthesis corresponds to the stability domain of apatite. A lower resolution observed for ν_3 and ν_4 phosphate absorption bands can also be pointed out from the vibrational spectra, which can be related to a lower crystallinity state (in accordance with XRD data) than for the AEP_r-free sample. It is interesting to recall here that such effects (nonstoichiometry witnessed by OH^- vacancies, lower crystallinity) are also commonly observed for biomimetic nanocrystalline apatites prepared at lower temperature and/or lower pH values.[30] Therefore, a comparison with the FTIR spectrum obtained with a less mature apatite sample appeared here of particular interest. For this comparison, a pure apatite sample corresponding to $x \sim 2$ was prepared (without stabilizing agent) at room temperature, under physiological pH and for a maturation time in solution of 3 h (see reported details on this synthesis route)[30] and its FTIR spectrum was recorded and added in Figure 6. As expected, a good accordance was seen, for the ν_3 and ν_4 absorption bands, with the spectrum of the colloidal apatite sample prepared with the starting ratio AEPr/Ca = 1.

In addition to the absorption bands related to this apatitic phase, some less intense absorption peaks are also observed, in particular, at 1530 and 754 cm^{-1}, as well as a large absorption band in the region 2700−3300 cm^{-1} (Figure 6). These absorptions cannot be assigned to apatite and are therefore likely linked to the presence of AEP_r in the system. In particular, the band observed at 754 cm^{-1} (Figure 6) has been attributed to the P−O−C bending vibration mode of AEP_r molecules.[31] In order to investigate this point, a comparison of the position of these bands was made with the FTIR spectra obtained with pure AEP_r as well as with its calcium salt $Ca(AEP_r)_2 \cdot nH_2O$ ($n \sim 2.8$) prepared by mixing (in water, neutral pH) calcium oxide and AEP_r in molar proportions 1:2 (see Figure 6) using a protocol previously reported in the literature.[32] Indeed, a previous work has suggested the presence of $Ca(AEP_r)_2$ surface complexes on apatite crystals prepared in the presence of AEP_r (at pH ~ 7 and following a different synthesis protocol).[18] As can be seen in Figure 6, a good match was found in the present work between the additional absorption bands observed for the colloid (beside those of apatite)

(30) Drouet, C.; Bosc, F.; Banu, M.; Largeot, C.; Combes, C.; Dechambre, G.; Estournes, C.; Raimbeaux, G.; Rey, C. *Powder Technol.* **2009**, *190*, 118–122.
(31) Zahidi, E. M. Ph.D. Thesis, *INP Toulouse*, France, **1984**.
(32) Bissinger, P.; Kumberger, O.; Schier, A. *Chem. Ber.* **1991**, *124*, 509–513.

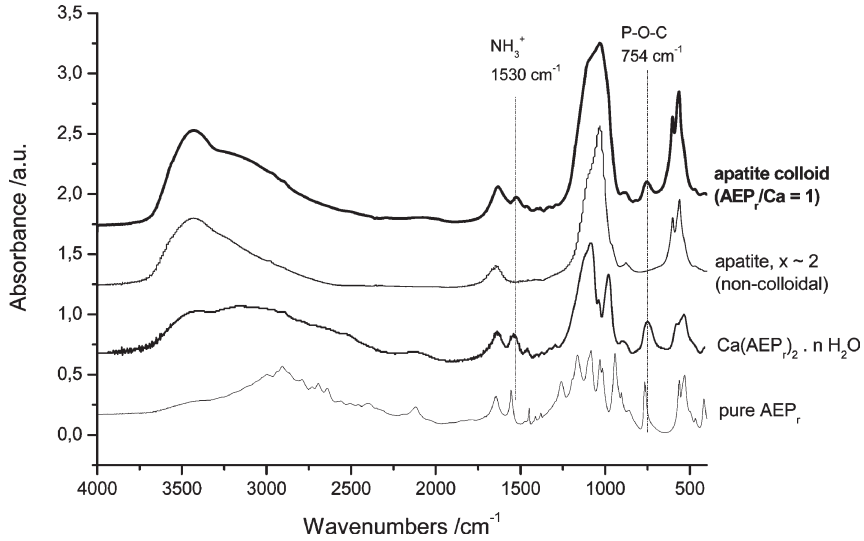

Figure 6. FTIR spectrum for apatite colloid obtained with $AEP_r/Ca = 1$, compared to three reference compounds: noncolloidal apatite sample with $x \sim 2$, AEP_r, and $Ca(AEP_r)_2 \cdot nH_2O$ ($n \sim 2.8$).

Table 1. Ionized Forms for AEP_r (Reported in Literature)[32]

pH scale	pH < 5.8	5.8 < pH < 10.5	pH > 10.5
ionized forms	$NH_3^+-CH_2-CH_2-OP(O)(OH)O^-$	$NH_3^+-CH_2-CH_2-OP(O)(O^-)_2$	$NH_2-CH_2-CH_2-OP(O)(O^-)_2$
overall charge	AEP_r^0	$AEP_r^{(-)}$	$AEP_r^{(2-)}$

Table 2. Compositional Evaluations for Freeze−Dried Apatite Colloids (Purified by Dialysis)

				for 1 g of (freeze−dried) colloid			
starting AEP_r/Ca molar ratio	wt % nitrogen in colloid	wt % AEP_r in colloid	final $Ca(AEP_r)_2$/apatite molar ratio in colloid	total calcium content (mmol)	mineral phosphate content (mmol)	AEP_r content (mmol)	value of "x" in apatite phase (from Raman data): $Ca_{10-x}(PO_4)_{6-x}(HPO_4)_x(OH)_{2-x}$
1	2.54	25.4	1.39	6.14	3.92	1.81	$x \sim 2$
0.6	2.30	23	1.28	5.94	3.84	1.64	$x \sim 2$
0.4	2.08	20.8	1.07	6.28	4.15	1.49	$x \sim 2$

and those of pure $Ca(AEP_r)_2 \cdot nH_2O$. On the contrary, only a poor correspondence with the spectrum of pure (separated) AEP_r molecules was seen. It is also noteworthy mentioning that the FTIR bands characteristic of $Ca(AEP_r)_2$ did not disappear after ultracentrifugation, which suggests the existence of a strong interaction between the apatite phase and a compound "close to" $Ca(AEP_r)_2$. Interestingly, the presence of a $Ca(AEP_r)_2 \cdot nH_2O$ phase was, however, not detected by XRD. Taking into account all these findings, the concept of $Ca^{2+}(AEP_r^-)_2$ bidentate surface complexes localized on the apatite nanocrystals appears therefore as the most plausible description for such colloids, which can also explain the downsize effect observed in the presence of AEP_r.

These considerations have also to be related to the pK_a values determined for AEP_r which show that, at our synthesis pH value close to 9, AEP_r molecules exhibit one overall negative charge (Table 1).[33] The semideveloped chemical formula of such AEP_r^- molecules is then $NH_3^+-CH_2-CH_2-O-P(O)(O^-)_2$ and the interaction with calcium ions can be undergone by a complexation with the phosphate end of these AEP_r^- molecules. Therefore, the presence of AEP_r^- on the surface of the colloidal particles should lead to a modification of their surface charge. In the present work, the zeta potential (at pH ~ 9) of such colloids was found to be close to $+25 \pm 4$ mV. This value indicates that the surface of the colloidal apatite particles is clearly positively charged at this pH value, in contrast with the negative surface potential classically observed in similar conditions for hydroxyapatite.[34] Moreover, the FTIR band observed at 1530 cm^{-1} (Figure 6) has been previously assigned to vibrations of the ammonium group $-NH_3^+$ rather than of neutral amine $-NH_2$ in the case of AEP_r molecules.[31]

All of these observations are thus in agreement with the presence of AEP_r^- molecules bound to calcium ions in $Ca(AEP_r)_2$ surface complexes as observed by FTIR and exhibiting positively charged amino groups to the periphery of the particles (ammonium groups $-NH_3^+$ spreading outward). The presence of such positively charged functional end-groups is thought to participate in the stabilization of the colloidal suspension through an electrostatic repulsive effect between adjacent particles.

The amount of AEP_r contained in this colloid (25.4 wt % AEP_r, corresponding to 29.0 wt/% $Ca(AEP_r)_2$) was evaluated (Table 2) from the measurement of the amount of nitrogen in the system (elemental microanalysis, relative error 0.4%). The total calcium content in the colloid was then measured, as well as the amount of mineral phosphate ions (as opposed to the organic phosphate groups contained in AEP_r). Interestingly, the overall Ca/P molar ratio determined experimentally for this colloid was found to be noticeably greater (> 1.5) than the value (1.33) corresponding to

(33) Christoffersen, J.; Christoffersen, M. R. *J. Cryst. Growth* **1981**, *53*, 42–54.

(34) Somasundaran, P.; Wang, Y. H. C. In *Adsorption on and surface chemistry of hydroxyapatite*, Misra, D.N., Ed.; Plenum Press: New York, 1984; p 129−149.

$Ca_{10-x}(PO_4)_{6-x}(HPO_4)_x(OH)_x$ with $x = 2$ ("x" value drawn above from FTIR and Raman data). This finding therefore unveils the presence in the colloid of "supplementary" Ca^{2+} ions (in addition to the calcium ions contained in the apatite phase). This can then be related to the above discussion, strongly suggesting that the $Ca(AEP_r)_2$ surface complexes located on apatite nanocrystals involve "extra" Ca^{2+} ions (sequestrated by AEP_r^- from the synthesis solution). Table 2 summarizes the compositional data evaluated for this colloid.

The possibility for some surface Ca^{2+} ions from apatite to be involved in the formation of some $Ca^{2+}(AEP_r^-)_2$ complexes was also considered. However, since the number of moles of apatite in the colloid ($n_{apatite}$) can be calculated as:

$$n_{apatite} = \frac{n_{Cainapatitephase}}{10-x} = \frac{1}{10-x} \cdot (n_{Catotal} - n_{supernumeraryCa}) \quad (2)$$

(where $(10 - x)$ still represents the amount of calcium per apatite unit formula, with x constrained in the range 0−2), then an increase of the number of Ca^{2+} ions from apatite involved in the formation of $Ca(AEP_r)_2$ complexes would lead to a decrease of the number of "supernumerary" Ca^{2+} ions (referred to in eq 2 as "$n_{supernumerary\ Ca}$"), in turn leading to an increase of the total number of moles of apatite in the colloid. Yet, this increase was found to lead to calculated $n_{apatite}$ values departing from the experimental value of $n_{apatite}$ (determined as one-sixth of the mineral phosphate content, since 1 mol of apatite contains 6 mol of phosphates) even when only a few percent of the apatite calcium ions were considered. This point, therefore, tends to show that the involvement of Ca^{2+} ions from the surface of apatite is negligible in the process of formation of the $Ca(AEP_r)_2$ complexes, uniquely involving "additional" Ca^{2+} ions. Considering the amount of "supplementary" calcium ions linked to the AEP_r molecules in $Ca(AEP_r)_2$, the calcium to (mineral) phosphorus molar ratio can be calculated from the data reported in Table 2, leading to Ca/P = 1.33(5), which is in very good agreement with the Raman data suggesting $x = 2$ in the apatite chemical formula.

3.2.2. Influence of the Concentration in AEP_r. In order to determine the influence of the concentration in AEP_r in the starting synthesis mixture, several additional samples were prepared with decreasing amounts of AEP_r, corresponding to initial AEP_r/Ca molar ratios of 0.6, 0.4, 0.2, and 0.1.

As for an AEP_r-free synthesis, the suspensions obtained with AEP_r/Ca = 0.1 and 0.2 were not stable and were prone to a progressive sedimentation. In contrast, suspensions prepared with the ratios 0.4 and 0.6 were stable colloids in a similar way as that observed for AEP_r/Ca = 1 (see previous section).

FTIR and XRD analyses for the stable colloids corresponding to AEP_r/Ca = 0.4 and 0.6 gave highly similar results to those for AEP_r/Ca = 1. In particular, no crystalline phase was identified by XRD besides apatite. Raman data also indicated very similar results to those for AEP_r/Ca = 1, namely, a nondetectable amount of OH^- ions in the apatite phase ($x \sim 2$).

The median particle size parameter d_{50} of such suspensions was determined and is given in Figure 7 (plain curve) as a function of the starting AEP_r/Ca ratio. This curve can be decomposed into two parts. It first shows a steep decrease of the particle size for increasing AEP_r/Ca ratios up to ca. 0.4. Beyond this value, a stabilization is observed, corresponding to a d_{50} size parameter close to 29 nm for an AEP_r/Ca ratio around 0.5. The first decrease demonstrates that the interactions, during synthesis, between AEP_r (or more specifically $Ca(AEP_r)_2$) and the forming apatite nanocrystals progressively intensify, and finally lead to stable colloids when the medium becomes sufficiently rich in AEP_r. For

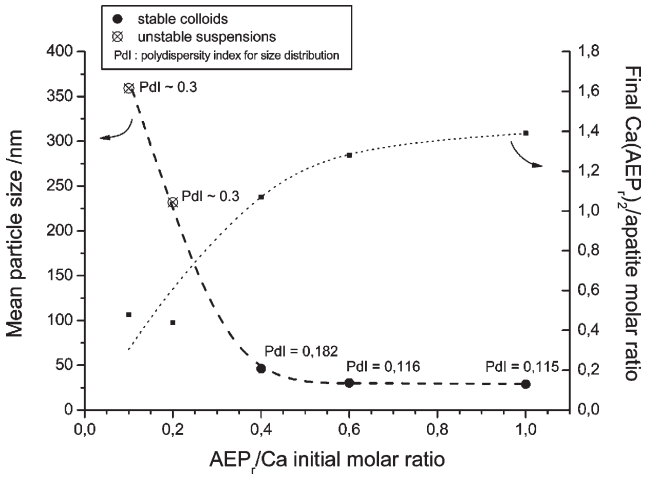

Figure 7. Effect of AEP_r/Ca initial molar ratio on particle size and final $Ca(AEP_r)_2$ content in the (purified) suspensions.

AEP_r/Ca ratios above 0.4, the effect of AEP_r concentration on particle size becomes much less pronounced and reaches a stabilization (beyond AEP_r/Ca ~ 0.5). It can be concluded from these results that a minimal amount of AEP_r is required during synthesis in order to stabilize the suspensions as colloids and to efficiently limit the size of the particles composing the suspension.

The value of the polydispersity index (PdI), giving a measure of the width of the granulometry distribution (derived from the autocorrelative function of the granulometry data) has also been followed and reported for each suspension in Figure 7. A noticeable decrease of this index, traducing the narrowing of the particle size distribution, is observed when increasing the initial concentration in AEP_r in the medium. It can most probably be related to a progressively more homogeneous distribution of $Ca(AEP_r)_2$ complexes on the surface of the apatite nanocrystals, therefore enabling an efficient and homogeneous control of the particle size through electrosteric hindrance effects.

Compositional results concerning the stable colloids corresponding to AEP_r/Ca = 0.4 and 0.6 were determined as previously and added in Table 2. As for the initial ratio AEP_r/Ca = 1, the best accord between experimental data and calculations was found when the amount of Ca^{2+} ions arising from apatite and involved in the formation of $Ca(AEP_r)_2$ complexes was neglected.

The amount of AEP_r molecules associated (as $Ca(AEP_r)_2$ surface complexes) with the apatite particles in unstable (sedimented) suspensions obtained from AEP_r/Ca = 0.1 and 0.2 was also evaluated for comparative purposes. The results obtained (Figure 7, dotted curve) show that the amount of AEP_r associated to the apatite nanoparticles increases steeply with the AEP_r/Ca ratio from 0.1 to ca. 0.5; above this value, a stabilization of the $Ca(AEP_r)_2$ content is observed. Interestingly, this trend coincides well with the observed decrease in particle size (Figure 7, plain curve). It could be assessed that the stabilization of the particle size to about 29 nm for AEP_r/Ca ratios greater than ca. 0.5 is linked to the progressive limitation of the number of accessible sites (in the room-temperature experimental conditions used here) for further associations with additional $Ca(AEP_r)_2$ surface complexes.

The morphology of such colloidal particles (for starting AEP_r/Ca ratios greater than 0.4) was then followed by TEM. A typical example is reported in Figure 8b (case of AEP_r/Ca = 1). The particles were found to exhibit a good morphological homogeneity throughout the samples, with mean sizes in good agreement with granulometry data (e.g., spheroidal particles with diameters

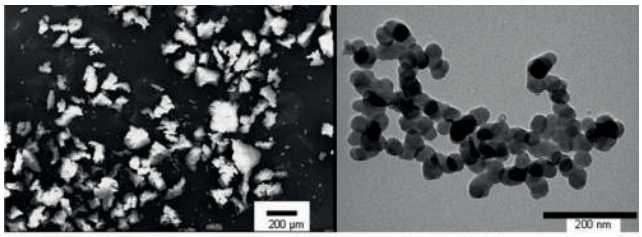

Figure 8. Electron microscopy observations for (a) noncolloidal "hap-ref" sample (SEM micrograph, 50×) and for (b) apatite colloid prepared from $AEP_r/Ca = 1$ at 80 °C for 16 h. aging (TEM micrograph, 200 000×).

close to 40 nm for Figure 8b), which also confirmed the values of the hydrodynamic radii drawn from dynamic light scattering experiments. In contrast, SEM observation of the noncolloidal, AEP_r-free sample "hap-ref" (Figure 8a) showed the absence of a definite morphology and a high heterogeneity in particle aspects, evidencing the strong agglomeration undergone by the constituting nanocrystals in the absence of efficient dispersing/stabilizing agents. The high homogeneity in particle aspects and sizes evidenced by TEM for the stable apatite colloids ($AEP_r/Ca \geq 0.4$) tends to confirm a homogeneous distribution of Ca^{2+}-$(AEP_r^-)_2$ complexes on the apatite nanocrystals throughout the colloids, which can also explain the efficient size-reducing effect observed by granulometry and the monomodal size distribution.

3.2.3. Influence of Temperature and Duration of the Aging Step. The synthesis route developed so far in this work to obtain apatite colloids included an aging step in an oven set to 80 °C for 16 h. It was shown above to lead to the preparation of stable colloids for initial molar ratios AEP_r/Ca above ca. 0.4, with a particle sizes well below 100 nm, ranging from 29 to 47 nm. It was however of interest to evaluate the influence on particle size of the temperature at which this step was performed, and also of its duration.

To this aim, additional experiments were run: (i) for 16 h but at varying aging temperatures (37, 60, and 100 °C) and (ii) at 80 °C but for several durations of the aging step (1, 2, 4, 6.5, and 8 h, and 8 days). For these experiments, the initial AEP_r/Ca ratio was fixed to 0.4, as this value was found above to lead to stable colloids and to be close from the stabilization point in particle size (when the suspension was aged at 80 °C for 16 h; see Figure 7).

The samples aged at temperatures 37 and 60 °C were found to exhibit a thick gel-like texture, in contrast to the fluid suspensions obtained at 80 or 100 °C. XRD analyses of the samples prepared at 37 or 60 °C showed mainly the presence of two large halos centered around $2\theta = 36°$ (major) and 56° (minor) (with $\lambda_{Co} = 1.788\,92$ Å). These halos are characteristic of amorphous calcium phosphate. These findings show that, at least for an aging step of 16 h, a temperature too low such as 37 or 60 °C reduces drastically the kinetics of crystallization (from amorphous calcium phosphate to apatite) and possibly also the rate of surface organization of $Ca(AEP_r)_2$ complexes, and are therefore not adapted to the preparation of fluid apatite colloids.

Interestingly, very similar results (compact gels, mostly amorphous calcium phosphate observed by XRD) were found for syntheses run at 80 °C for aging steps of 1, 2, 4, or 6.5 h. On the contrary, stable and fluid suspensions were obtained after 8 h or 8 days of aging at 80 °C, as was previously observed for 16 h. These findings indicate that a sufficient amount of time is needed, at a given temperature (e.g., 80 °C), for the calcium phosphate/AEP_r system to arrange into a stable colloid.

Table 3. Median d_{50} Size Parameter for Apatite Colloids Prepared in Varying Conditions

aging step				
temperature	duration	pH	sonication prior to aging	d_{50} size parameter (nm)
		$AEP_r/Ca = 0.4$		
80 °C	16 h	9	-	46
100 °C	16 h	9	-	40
80 °C	8 h	9	-	70
80 °C	8 days	9	-	39
80 °C	16 h	7	-	116
80 °C	16 h	9	15 min	34
		$AEP_r/Ca = 0.6$		
80 °C	16 h	9	-	31
		$AEP_r/Ca = 1$		
80 °C	16 h	9	-	29

The above findings illustrate the impact of the temperature and duration of the aging step on the thermodynamic and kinetic rules governing the crystallization process occurring during heating (in the presence of AEP_r), and probably also the process by which the $Ca(AEP_r)_2$ complexes can accumulate in a stable way on the surface of apatite nanocrystals.

The influence of the temperature and duration of aging on the mean particle size was followed in the cases when fluid suspensions were obtained (Table 3). For the sake of completeness, the mean particle sizes reported previously in the text for other Ca/P ratios (0.6 and 1) have also been added in this table.

The average d_{50} size parameter corresponding to the sample aged at 100 °C for 16 h was found to be slightly lower (40 nm) than for the sample prepared at 80 °C for 16 h (46.4 nm). A rather similar decrease in size was also observed for the suspension aged for 8 days at 80 °C (39 nm) as compared to 16 h (46 nm). These findings show in both cases a decrease in particle size close to 15%, and therefore point out the potential impact of an increased temperature and of a lengthened aging step on the limitation of the final particle size in the colloid. These parameters could thus be exploited further, in view of the production of size-controlled apatite colloids, typically in the range 30−100 nm, as needed for specific applications.

The fluid suspension obtained after aging for 8 h led, on the other hand, to a d_{50} parameter around 70 nm, clearly higher than after 16 h of aging. This point shows the interest in leaving the suspensions for an aging period sufficiently long to limit the particle size in the final suspension. The plot of the particle size versus the duration of aging (not shown here for the sake of brevity), based on the data points of this work, suggests that a stabilization of the particle size to its minimum would be expected after ca. 45 h of aging (at 80 °C).

These data could, at first glance, seem surprising when compared to results obtained for the precipitation of apatites in the absence of dispersing agents, where an increase of the duration and/or temperature of maturation in solution tends to lead to bigger constitutive crystals. However, it should be reminded here that the presence of AEP_r enables limitation of the agglomeration of adjacent crystals (leading in optimal conditions to individualized nanocrystals), whereas a strong agglomeration effect is always observed for apatites precipitated without dispersing agents. What is being measured in this work is the size of the particles (thus possibly agglomerated). Therefore, it is possible to observe an overall decrease in particle size despite some

simultaneous crystal growth; the presence of a dispersing agent such as AEP_r in the system is indeed bound to modify the behavior of the particles, in particular by changing the relative impact of several concomitant phenomena: the agglomeration process (especially for very immature samples showing a high surface energy) as well as the crystal growth and surface reactivity with AEP_r molecules. This point will be discussed further in the next section.

3.2.4. Influence of Starting pH. The above-mentioned suspensions were prepared with a starting pH value of 9 in order to orient the synthesis toward the formation of a hydroxylated apatite phase, thermodynamically more stable and better crystallized than usual biomimetic apatites generally prepared for other applications (e.g., bone tissue engineering). In order to study, however, the influence of the initial pH value on the physicochemical characteristics of the colloids obtained, a synthesis was run with an initial pH set to 7, at 80 °C for 16 h, and corresponding to the starting ratio $Ca/AEP_r = 0.4$.

XRD and FTIR analyses on this sample prepared at pH = 7 showed similar results as previously, with apatite being the only crystalline phase identifiable by XRD and with vibrations from $Ca(AEP_r)_2$ clearly visible by FTIR.

Although a stable colloid was also obtained at pH = 7, a noticeable increase of the d_{50} size parameter was observed (close to 116 nm) as compared to the suspensions prepared at pH = 9. Both the pH values 7 and 9 are, however, found in a pH region where the AEP_r molecule is stable in its monovalent anionic form AEP_r^- (considering the pK_a values reported; see Table 1).[33] Therefore, the agglomeration effect cannot be related to a change in speciation of the AEP_r molecules, and probably originates from modifications of the internal organization of the apatite/$Ca(AEP_r)_2$ system.

The results obtained in the previous sections of this article have shown that a lowering of the temperature and/or of the duration of the aging step led to an increase of the mean particle size and of the viscosity of the suspension (with the formation of a gel observed in some conditions). Considering the above findings, a lowering of the starting pH value from 9 to 7 also seems to have similar consequences.

Interestingly, those three parameters (temperature, duration of aging/maturation in solution, and pH) have been shown in previous works related to nanocrystalline apatite compounds to strongly affect the physicochemical characteristics of apatite nanocrystals precipitated in aqueous media.[30] Indeed, a decrease in the synthesis temperature, maturation time, and/or pH (in the limit of the stability of the apatite phase) was found to lead to less mature apatite nanocrystals, exhibiting a lower degree of crystallinity and a greater amount of crystallographic vacancies. The XRD analysis performed here for the sample prepared at pH = 7 confirmed the lower degree of crystallinity (broader diffraction lines) than for samples prepared at pH = 9, and these results are thus indicative of a less mature apatite phase.

Literature reports showed that immature calcium phosphate apatites were composed of plate-like nanocrystals exhibiting high surface areas and the presence of a hydrated layer observed on the nanocrystals is thought to contribute to decrease the high surface energy of the system.[35,36] For very immature apatites, a strong agglomeration of the nanocrystals generally occurs, since agglomeration is a way to reduce the overall surface energy.

The data reported in the present contribution on apatite-based colloids containing AEP_r showed that experimental conditions favoring the preparation of immature apatite (decreased temperature, aging duration, and/or pH) led to an increase in the size of the particles (agglomerates) constituting the suspensions. This increase in size can be explained by a less efficient interaction between very immature apatite nanocrystals and AEP_r (as $Ca(AEP_r)_2$ surface complexes involving "supernumerary" Ca^{2+} ions). This phenomenon can most probably be linked to the high surface energy of highly immature apatite nanocrystals exhibiting a strong tendency to agglomerate as soon as they form, at the expense of a more complex and efficient interaction with $AEP_r/Ca(AEP_r)_2$ complexes. In this case, the thermodynamic stabilization gained through the agglomeration process could then prevail on the formation of colloidal particles, despite their electrosteric repulsive effect and Brownian motion. This explanation is also supported by the fact that the sample (initial AEP_r/Ca ratio: 0.4) prepared at pH = 7 shows a final $Ca(AEP_r)_2$/apatite molar ratio (0.34) markedly lower than for pH = 9 (ratio 1.07), therefore pointing out a much lower degree of interaction between apatite and $Ca(AEP_r)_2$.

The above findings on the effect of the starting pH value showed that an alkaline pH of 9 was well-adapted to the preparation of apatite colloidal nanoparticles noticeably smaller than 100 nm, in contrast to an initially neutral pH leading to substantially larger nanoparticles. However, considering the biological applications intended for such colloids, the need to obtain in the end neutral suspensions is primordial. It is interesting to remark that this goal was achieved, with a conserved stability, in this work by proceeding to a neutralization step after preparing the colloids at pH 9.

3.2.5. Influence of Sonication Prior to Aging. The above discussion shows that the natural tendency of apatite nanocrystals to agglomerate is a major parameter to consider in view of obtaining colloidal apatitic suspensions with particles smaller than 100 nm. Therefore, the limitation of the initial agglomeration occurring at the beginning of the synthesis could potentially facilitate the association between apatite and $AEP_r/Ca(AEP_r)_2$ complexes. One way to limit this initial agglomeration is by incorporating a sonication treatment (generation of ultrasounds) during the 15 min that follow the mixing of the starting solutions (before aging).

The d_{50} size parameter obtained with a sonication treatment (500W sonication probe, amplification rate: 70%) in the case of a starting AEP_r/Ca ratio of 0.4 was 34 nm. Although the effect of sonication has not been thoroughly investigated here, this value clearly falls below the one (46 nm) obtained in the same conditions without sonication, and this difference is beyond experimental error. It therefore unveils the potential interest of sonication for limiting the initial agglomeration stage for apatite nanocrystals, during the first minutes of precipitation in the presence of AEP_r, and could thus be seen as another experimental parameter, besides temperature and aging time, to tailor the size of apatite colloidal nanoparticles.

3.2.6. Final Statements and Perspectives. The results reported in this contribution revealed the possibility to prepare stable fully biocompatible apatite-based colloids, from easily handled nontoxic starting materials. Also, we showed the possibility to tailor the nanoparticles size in a rather narrow monomodal size distribution, with mean sizes typically controllable in the range 30−100 nm, so as to adapt to selected intracellular drug delivery requirements.

(35) Eichert, D.; Drouet, C.; Sfihi, H.; Rey, C.; Combes, C. In *Biomaterials Research Advances*, Kendall, J. B., Ed.; Nova Science Publishers: New York, 2007; p 93−143.

(36) Cazalbou, S.; Eichert, D.; Drouet, C.; Combes, C.; Rey, C. *C. R. Palevol.* **2004**, *3*, 563–572.

The possibility to associate (noncolloidal) apatite nanocrystals and drugs (or other active agents) has already been shown.[37] Such an association is especially favorable when the organic drugs/molecules exhibit at least one charged functional group which is bound to interact with the apatite surface, either during the apatite precipitation/aging stages or in a subsequent step. Consequently, the idea to "load" apatite-based colloids such as those prepared in this work with various types of drugs appears as a promising perspective, which is now under investigation.

For illustrating this aspect, preliminary experiments were carried out here by adding folic acid (concentration tested: 200 ppm) directly to the precipitating system (corresponding to the starting molar ratios $AEP_r/Ca = 1$) prior to aging at 80 or 100 °C for 16 h, since the stability of folic acid at these temperatures was previously checked even in the dry state.[38] Contrary to the experiment mentioned in a previous section of this contribution and relating to the search for potential stabilizing properties of folic acid, the experiment described here involved the presence of both AEP_r (for efficient stabilization of the colloid) and folic acid. In these conditions, the interaction with folic acid did not lead to sedimentation. In contrast, stable fluid colloids were obtained indicating that the efficacy of stabilization ensured by AEP_r molecules still remained. As found earlier for AEP_r, our results showed that the presence of folic acid (leading to a characteristic yellow coloration to the powder) was conserved even after ultracentrifugation with successive washing steps. The presence of folic acid after ultracentrifugation was then further confirmed by UV−visible absorption, where a peak at 256 nm characteristic of folic acid[39] was clearly evidenced. This observation suggests a close interaction between the molecules of folic acid and the colloidal apatite particles, probably via grafting on Ca^{2+} ions available on the surface of the particles. These data are particularly interesting since the folic acid molecule presents strong compositional analogies with methotrexate (CAS number: 59−05−2), an anticancer drug used to treat, for example, breast, bladder, and bone cancers; thus making folic acid a good model in preliminary studies for mimicking the chemical interaction of methotrexate with propitious substrates/carriers. This consideration is all the more appropriate, as the sole modifications existing between the molecules of folic acid and of methotrexate occur in the "biologically-active head" of the molecules (pterin derivatives) and not in the "attachment head" (resembling glutamic acid), which is the same for both molecules.

These observations illustrate the possibility of regarding biomimetic apatite colloids as potential nanocarriers for drug delivery, especially recalling that biomimetic apatites should readily dissolve (thus decomposing into natural ionic metabolites and simultaneously liberating the carried drug) after endocytosis due to the acidic conditions ($pH < 6$) reigning in the endosomes and lysosomes of the hosting cells.[40] Such an acidic dissolution has indeed already been observed for (noncolloidal) hydroxyapatite samples on several cell types, including, for example, human fibroblasts.[41,42]

The perspectives of this work are now being considered for examining, from a biological viewpoint, the advantages and limitations of such systems.

4. Conclusions

Biomimetic calcium phosphate apatite-based suspensions were produced starting from easily handled, nontoxic ionic salts and using several potential dispersing/stabilizing agents. Among the agents tested, 2-aminoethylphosphoric acid (AEP_r), a natural phospholipid moiety, was found to stabilize durably the suspensions for initial AEP_r/Ca molar ratios above 0.4.

Complementary physicochemical investigations strongly suggested that the colloids were composed of biomimetic apatite nanocrystals covered with $Ca^{2+}(AEP_r^-)_2$ surface complexes involving "supernumerary" Ca^{2+} ions. The impact of various synthesis parameters (concentration in AEP_r, temperature and duration of aging, starting pH, sonication) on the physicochemical characteristics of the colloids was investigated and discussed.

The mean size of such colloidal nanoparticles can be adjusted by modifying appropriately the synthesis conditions, which should facilitate the internalization of such particles by cells. These perfectly biocompatible systems (associating biomimetic apatites analogous to bone mineral and a phospholipid moiety), allied to the possibility to obtain them from easily handled, innocuous starting salts now advances growing perspectives in the field of cell-based therapeutics, for example, for delivering chemotherapeutic drugs. These aspects are now under consideration.

Supporting Information Available: TEM micrographs, granulometry results, and spectroscopic data. This material is available free of charge via the Internet at http://pubs.acs.org.

(37) Chowdhury, E. H.; Akaike, T. *J. Controlled Release* **2006**, *116*, e42–e43.
(38) Vora, A.; Riga, A.; Dollimore, D.; Alexander, K. *J. Therm. Anal. Calorim.* **2004**, *75*, 709–717.
(39) Sculthorpe, N. F.; Davies, B.; Ashton, T.; Allison, S.; Mc Guire, D. N.; Malhi, J. S. *J. Public Health Med.* **2001**, *23*, 195–197.
(40) Day, B. P. F.; Gregory, J. F. *J. Food Sci.* **1983**, *48*, 581–599.
(41) Bonifacino, J. S.; Traub, L. M. *Annu. Rev. Biochem.* **2003**, *72*, 395–447.
(42) Cheung, H. S.; McCarty, D. J. *Exp. Cell Res.* **1985**, *157*, 63–70.